1-1-2003

Subsurface maxima of phytoplankton and chlorophyll: Steady-state solutions from a simple model

Katja Fennel
Rutgers University–New Brunswick

Emmanuel Boss
University of Maine, emmanuel.boss@maine.edu

Limnol. Oceanogr., 48(4), 2003, 1521–1534

Subsurface maxima of phytoplankton and chlorophyll: Steady-state solutions from a simple model

Katja Fennel[1]
Institute of Marine and Coastal Sciences, Rutgers University, New Brunswick, New Jersey

Emmanuel Boss
School of Marine Sciences, University of Maine, Orono, Maine

Abstract

In oligotrophic lakes and oceans, the deep chlorophyll maximum may form independently of a maximum of phytoplankton biomass, because the ratio of chlorophyll to phytoplankton biomass (in units of carbon) increases with acclimation to reduced light and increased nutrient supply at depth. Optical data (beam attenuation as proxy for phytoplankton biomass and chlorophyll fluorescence and absorption as proxies for chlorophyll concentration) and conventional measurements of biovolume, particulate organic carbon, and chlorophyll from two oligotrophic systems (Crater Lake, Oregon, and Sta. ALOHA in the subtropical North Pacific Ocean) are presented and show a vertical separation of the maxima of biomass and chlorophyll by 50–80 m during stratified conditions. We use a simple mathematical framework to describe the vertical structure of phytoplankton biomass, nutrients, and chlorophyll and to explore what processes contribute to the generation of vertical maxima. Consistent with the observations, the model suggests that biomass and chlorophyll maxima in stable environments are generated by fundamentally different mechanisms. Maxima in phytoplankton biomass occur where the growth rate is balanced by losses (respiration and grazing) and the divergence in sinking velocity, whereas the vertical distribution of chlorophyll is strongly determined by photoacclimation. A deep chlorophyll maximum is predicted well below the particle maximum by the model. As an interpretation of these results, we suggest a quantitative criterion for the observed coexistence of vertically distinct phytoplankton assemblages in oligotrophic systems: the vertical position at which a species occurs in highest abundance in the water column is determined by the ''general compensation depth''—that is, the depth at which specific growth and all loss rates, including the divergence of sinking/swimming and vertical mixing, balance. This prediction can be tested in the environment when the divergence of sinking and swimming is negligible.

Subsurface maxima of phytoplankton biomass and/or chlorophyll often occur in clear waters in the ocean and in lakes—for example, the deep chlorophyll maximum at the base of the euphotic zone is a ubiquitous feature (Riley et al. 1949; Steele and Yentsch 1960; Venrick et al. 1973; Cullen and Eppley 1981; Cullen 1982). A basic understanding of the generating mechanisms for these vertical maxima is important for the assessment of the functioning of the pelagic food web and for the application of remote sensing techniques to infer vertically integrated values of biomass and primary productivity. Current textbooks in biological oceanography (e.g., Jumars 1993; Mann and Lazier 1996) do not provide a consistent explanation for the existence of subsurface pigment and/or phytoplankton biomass maxima. In the present article, we provide a mathematical framework that is consistent with observations and revisit explanations that have been given in the past. Our approach is based largely on the insightful analyses of Riley et al. (1949), Steele and Yentsch (1960), and Steele (1964), three important studies that unfortunately have been largely ignored.

A variety of different explanations for the creation and maintenance of subsurface maxima of phytoplankton biomass or chlorophyll have been given since the 1950s (*see* Cullen 1982). Riley et al. (1949) combined photosynthesis, respiration, grazing, and sinking in a simple mathematical model to describe the vertical structure of phytoplankton biomass, with no clear distinction made between phytoplankton biomass and chlorophyll. The model produced subsurface phytoplankton maxima at or above the daily mean compensation depth (where growth and community respiration rates balance, significantly above the observed deep chlorophyll maximum). A number of studies focused on a reduction of the sinking velocity with depth as a mechanism that could result in vertical maxima of biomass below the compensation depth at the base of the euphotic zone (Steele and Yentsch 1960; Lerman et al. 1974; Bienfang et al. 1983). Steele and Yentsch (1960) suggested a reduction of the sinking rate in the dark, nutrient-rich waters near the nutricline. Bienfang et al. (1983) reported that low light levels alone could reduce the sinking velocity. Lerman et al. (1974) suggested a decrease in the sinking velocity with depth due to dissolution of the sinking particles.

In 1964, Steele postulated a qualitatively different, physiological mechanism for the creation of the deep chlorophyll

[1] Corresponding author (kfennel@imcs.rutgers.edu).

Acknowledgments

We thank the HOT program PIs and personnel and Gary Larson and the Crater Lake Limnological Study personnel for providing data and expertise. Discussions with R. Letelier, M. J. Perry, and M. Behrenfeld are gratefully acknowledged. A very detailed review by John Cullen and critical comments from John Steele and André Morel were greatly appreciated and helped improve an earlier version of the manuscript. Funding was provided by the U.S. Geological Survey to K.F. and E.B. and the Environmental Optics division of the Office of Naval Research to E.B.

maximum. He argued that sinking is unlikely to be an important factor in the oligotrophic ocean, where phytoplankton are often motile and where large downward fluxes by sinking particles appear as an inefficient response to the stable, nutrient-limited conditions. He suggested that, in those oligotrophic waters, the chlorophyll maximum does not represent a biomass maximum but is due to increased chlorophyll per biomass at low light levels (i.e., photoacclimation of phytoplankton), and he presented supporting data from the Gulf of Mexico.

Recent advances in optical measurements provide high-resolution profiles of beam attenuation and chlorophyll fluorescence and absorption. The beam attenuation has been used as a proxy of particulate organic carbon (POC; e.g., Bishop 1999; Gardner et al. 2000), and chlorophyll fluorescence and absorption have been used as proxies of chlorophyll concentration (e.g., Cullen 1982). These new data confirm that a subsurface particle maximum often exists separated from the deep chlorophyll maximum (Pak et al. 1988; Kitchen and Zaneveld 1990).

Here, we present data that demonstrate the existence and separation of persistent vertical particle and chlorophyll maxima in two stable environments: Crater Lake, Oregon, and Sta. ALOHA in the Pacific Ocean. We revisit the different explanations for the vertical distributions of phytoplankton biomass and chlorophyll concentration and suggest that the mechanisms for the maintenance of the deep chlorophyll maximum and the subsurface particle maxima in clear waters are fundamentally different. Following the methods of Riley et al. (1949), Steele and Yentsch (1960), and Steele (1964), we use a phytoplankton conservation equation that allows the inspection of the different mechanisms responsible for a vertical maximum of phytoplankton biomass. We add a nutrient conservation equation, to show how the dynamics of nutrients may influence the phytoplankton distribution. The addition of a photoacclimation model provides a mechanism for the creation of a chlorophyll maximum separated from the phytoplankton maximum. We support our conclusions by qualitative comparisons with field data and demonstrate that the basic features of the vertical distribution of phytoplankton particles, chlorophyll, and dissolved nutrients are captured in our simple model.

Materials and methods

Data—Optical measurements of in vivo fluorescence or absorption and beam attenuation can yield estimates of phytoplankton pigment concentrations and POC concentrations with much higher vertical and temporal resolution than conventional bottle determinations alone. Fluorescence and absorption are frequently used to determine chlorophyll concentrations (see below). Transmissometer measurements of the beam attenuation have been used successfully in a number of studies to estimate POC concentrations in the open ocean (see below).

At Sta. 13 in Crater Lake, measurements of beam attenuation and chlorophyll absorption were made during June and September 2001. Using a 25-cm path-length WetLabs ac-9, we measured beam attenuation by particles at 650 nm and estimated the chlorophyll concentration from the difference in absorption at 676 and 650 nm (Davis et al. 1997; Chang and Dickey 2001). Conventional measurements of phytoplankton biovolume and chlorophyll concentration were obtained from bottle samples as described in McIntire et al. (1996) and are available for biweekly periods from 1989 to 2000 for June–September. Measurements of nitrate and organic nitrogen were obtained as described in Larson et al. (1996) for the same period.

At Sta. ALOHA in the subtropical North Pacific, beam attenuation measurements were made between August 1991 and July 1995 using a SeaTech 25-cm path-length transmissometer measuring at 660 nm. In vivo fluorescence data, bottle determinations of chlorophyll, POC, nitrate, and dissolved organic nitrogen (DON), and measurements of primary production are available for the same period on a nearly monthly basis (e.g., Letelier et al. 1996). For these data, we establish relationships between the beam attenuation and the POC measurements from the bottle samples and between the in vivo fluorescence and bottle determinations of chlorophyll, respectively.

Fluorescence, absorption, and chlorophyll—Ideally, fluorescence and absorption would be expected to increase linearly with chlorophyll concentration. In reality, however, fluorescence per unit of chlorophyll varies in response to changes in nutritional status of phytoplankton, species composition, and time of the day. Fluorescence represents a small and variable fraction of the light absorbed by the photosynthetic apparatus. The fluorescence yield (the ratio of fluorescence to absorption) is very responsive to the ambient light and can change rapidly when shifts in irradiance are experienced by the phytoplankton (e.g., Cullen 1982). Nonphotochemical quenching of fluorescence has been observed near the surface, and diurnal changes occur (e.g., Falkowski and Raven 1997, their fig. 9.6). Absorption of chlorophyll does not suffer from nonphotochemical quenching. For many processes, including primary production, the in vivo pigment absorption (including packaging) is the relevant measure, as opposed to the extracted pigment concentration.

Pairs of fluorescence and extracted chlorophyll data, measured between August 1991 and July 1995 at Sta. ALOHA, are shown in Fig. 1. To account for possible changes in the instrument performance (due to changes in either its mechanical properties or the electronics), a vicarious calibration was performed in which all profiles were corrected by subtracting the mean signal over the 250–300 m depth interval. This procedure changes the calibration offset but does not affect the multiplicative constant provided by the manufacturer (which may have also changed). The extracted chlorophyll *a* data were determined by the fluorometric method. The data points appear to be grouped in two distinct branches in the fluorescence-chlorophyll phase plane, representing data from above and below the fluorescence maximum. This grouping might be due to an underestimation of extracted chlorophyll at depth by the fluorometric method, which occurs in the presence of chlorophyll *b* (Gibbs 1979; B. Bidigare pers. comm.). Using a robust linear regression model (geometric mean model II; Laws 1997), we found fluores-

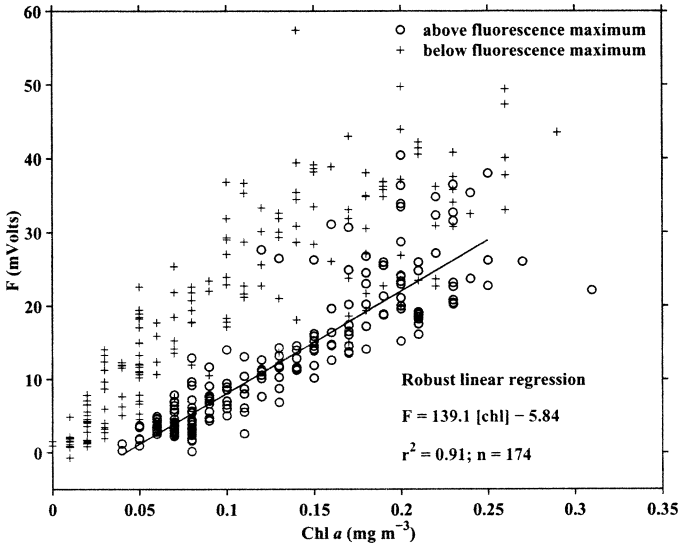

Fig. 1. Fluorescence versus bottle chlorophyll concentration at Sta. ALOHA. The regression for data above 120 m depth is given.

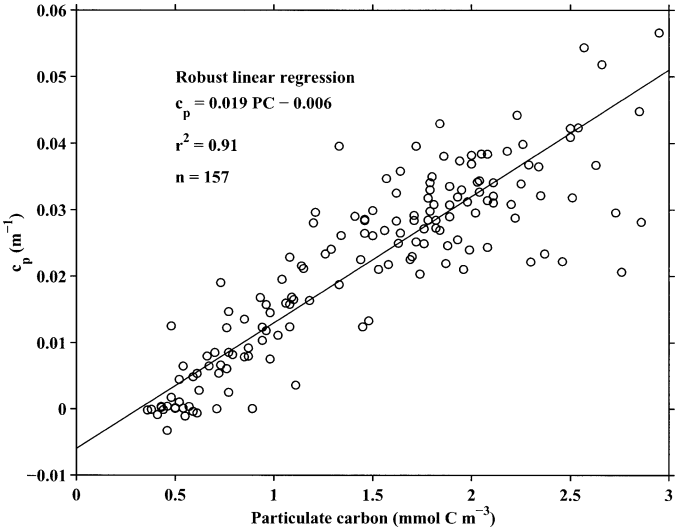

Fig. 2. Beam attenuation coefficient versus POC bottle concentrations at Sta. ALOHA and regression.

cence and bottle chlorophyll to be highly correlated (r^2 = 0.91) above the chlorophyll maximum (120 m) (Fig. 1).

Beam attenuation and particulate organic matter—The beam attenuation coefficient c is the sum of two dominant components, attenuation due to particles, c_p, and attenuation due to water, c_w (Zaneveld et al. 1994). c_w is constant, and its contribution is usually subtracted from c to obtain c_p. Calibrations of c_p versus bulk measurements of POC gave good linear correlations (e.g., Gardner et al. 2000), but there is no universal correlation between POC and c_p. Published POC versus c_p relationships show variability that can be introduced by variations in particle size distribution or composition (e.g., Morel 1973; Boss et al. 2001).

We determined c_p from the measured beam attenuation profiles by subtracting the mean value of beam attenuation over the depth interval from 250–300 m, which we consider as being representative of the beam attenuation value of particle free water (this value can be interpreted as a depth-independent, nonphytoplankton, background value). In all cases, the determined mean values were close to the value for particle-free water (as per calibration of the Sea-Tech transmissometer). The correlation between c_p and bottle measurements of POC was examined using a robust linear regression routine (geometric mean model II; Laws 1997). c_p and POC are highly correlated (r^2 = 0.91, Fig. 2), with a relationship that lies in the range of previously reported relationships (Table 1).

Results

Illustrative examples—Profiles of density, inorganic and dissolved organic nitrogen, beam attenuation and POC, and chlorophyll fluorescence and concentration at Sta. ALOHA (North Pacific) are shown in Fig. 3. Figure 4 shows profiles of density, beam attenuation, and chlorophyll absorption at Sta. 13 in Crater Lake.

At Sta. ALOHA, the water column is stratified with a weak pycnocline at 50 m depth (Fig. 3). Nitrate is depleted in the upper water column and starts to increase at 140 m depth. The DON is high in the upper water column (~5 mmol N m^{-3}). Despite the low nitrate concentrations, POC is high in the upper 80 m (~2 mmol C m^{-3}) and decreases below 80 m (to ~1 mmol C m^{-3} at the fluorescence maximum). The beam attenuation shows a maximum at 50 m depth. The chlorophyll concentration and fluorescence are low at the surface and increase with depth. The maximum chlorophyll concentration is located at 100 m depth, whereas the chlorophyll fluorescence is at maximum at ~120 m. Note that the relationship between the chlorophyll concentration and fluorescence changes below the maximum of chlorophyll concentration (*see Materials and Methods*).

In Crater Lake, the vertical stratification is weaker than that at Sta. ALOHA (Fig. 4). A pycnocline exists at 20 m

Table 1. Our regression $c_p = a\text{POC} + b$ in comparison with other published relationships.

Location	Slope a [m^{-1}(mmol C m^{-3})$^{-1}$]	Intercept b (m^{-1})
Station ALOHA (present study)	0.019	−0.006
Equatorial Pacific (Bishop 1999)	0.006	0.010*
Subarctic Pacific (Bishop et al. 1999)	0.006	0.005*
Arabian Sea (Gunderson et al. 1998)†	0.031	−0.007
Southern Ocean (Gardner et al. 2000)†	0.019	0.010

* Published relationship contains attenuation component due to water. For this comparison, 0.358 m^{-1} was subtracted

† Independent relationships were determined for different cruises. Values are given for the summer cruise in the Southern Ocean and the late northeastern monsoon period in the Arabian Sea.

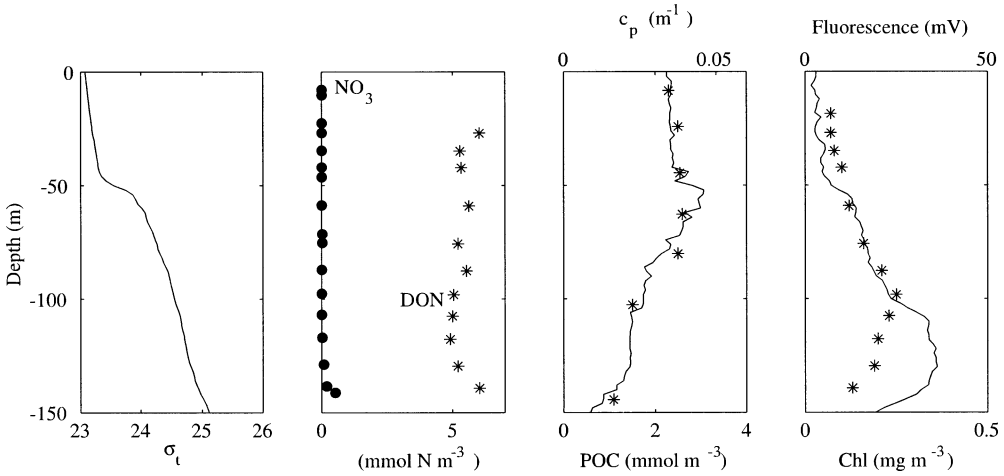

Fig. 3. Vertical profiles of density, nitrate and DON, beam attenuation c_p (solid line), POC (asterisks), fluorescence (solid line), and chlorophyll concentration (asterisks) at Sta. ALOHA on 9 August 1991.

depth. In June, a pronounced maximum in beam attenuation occurs at ~80 m depth, and the maximum of chlorophyll absorption is located at 150 m depth (Fig. 4, upper panels). In September, the beam attenuation is at maximum at 80 m depth, and a second maximum exists in the upper 20 m of the water column. The chlorophyll maximum is located at 130 m (Fig. 4, lower panels). Nitrate is depleted in the upper 200 m in June and in the upper 100 m in September. Estimates of the DON concentration from deep-water measurements of organic nitrogen yield a value of 0.7 mmol N m^{-3} (Larson et al. 1996).

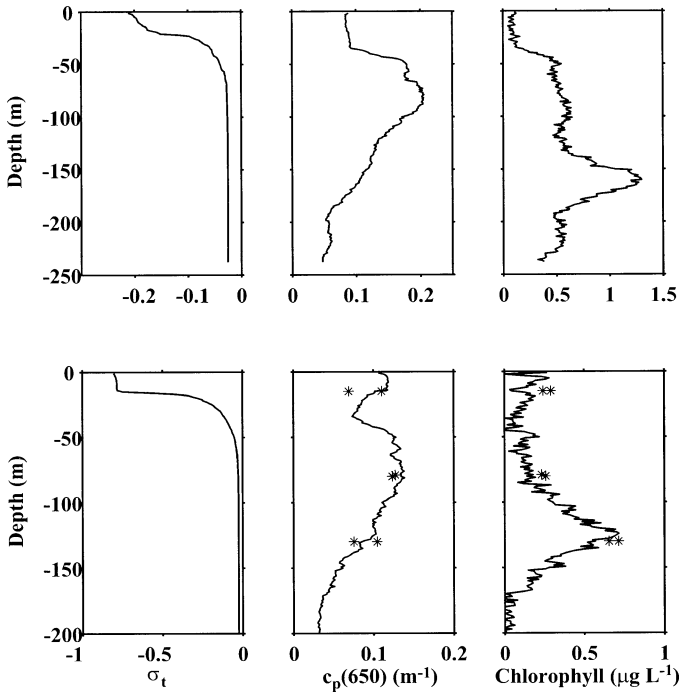

Fig. 4. Vertical profiles of density, beam attenuation c_p, particulate matter (asterisks), absorption-based chlorophyll, and extracted chlorophyll (asterisks) in Crater Lake on 28 June (upper panels) and 19 September (lower panels) 2001.

In the above examples, the vertical maxima of chlorophyll fluorescence/absorption and beam attenuation are separated by 50–70 m, and beam attenuation is highest in the upper 80 m of the water column. We argue that the vertical structure of phytoplankton biomass (in units of carbon) can be inferred from the vertical distribution of beam attenuation (proxy for POC) and that these examples show typical vertical distributions of phytoplankton biomass and chlorophyll in oligotrophic systems with a stable water column.

POC includes, in addition to phytoplankton carbon, the carbon biomass fractions of zooplankton, heterotrophic bacteria, and detritus. The relative contributions of phytoplankton, zooplankton, bacteria, and detritus to POC are hard to separate in measurements, because the different functional groups overlap in size. Optical measurements of the shape of the absorption spectrum could potentially help to separate the algal and nonalgal fraction of POC (Morrow et al. 1989; Roesler et al. 1989). Although we note that changes in the ratio of algal to nonalgal carbon may contribute to variation in the Chl : POC ratio (e.g., Loisel and Morel 1998), we neglect this component in the following discussion and assume that the vertical distribution of POC resembles that of phytoplankton biomass at Sta. ALOHA. Reported values for the contribution of phytoplankton carbon to POC range from ~30% (Beers et al. 1975; picoplankton not included) and 50% (Eppley et al. 1988) to 70% (Letelier et al. 1996) for the subtropical North Pacific and average 33% at the Bermuda time-series station in the North Atlantic (DuRand et al. 2001). At Sta. 13 in Crater Lake, time-series data of phytoplankton biovolume are available and allow a direct comparison of phytoplankton biomass and chlorophyll (*see Fig. 7 below*). The vertical distribution of biovolume is similar to the beam attenuation and POC profiles shown in Fig. 4.

The vertical structure of particulate matter, chlorophyll, and the chl : C ratio—We now analyze the vertical structure

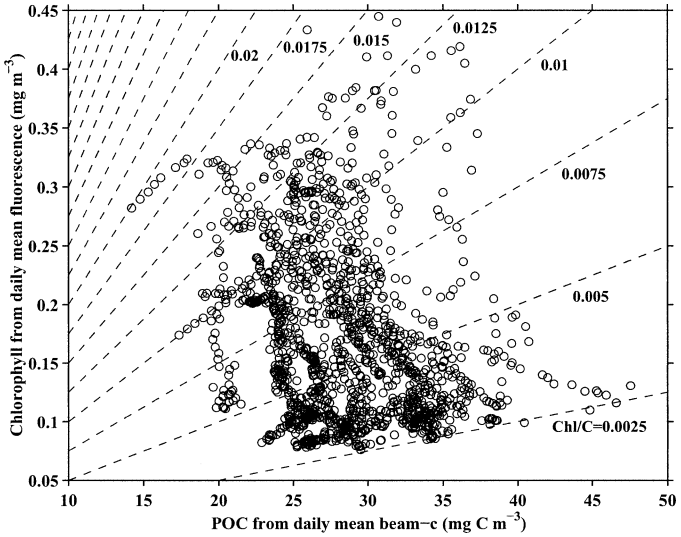

Fig. 5. Chlorophyll versus POC concentrations at Sta. ALOHA. Isolines of Chl : POC in g Chl (g C)$^{-1}$ are given as dashed lines. Chlorophyll and POC concentrations were obtained from daily mean profiles of fluorescence and beam attenuation. Each profile represents an average of ~10 casts. Data collected between August 1991 and July 1995 in the upper 120 m are shown.

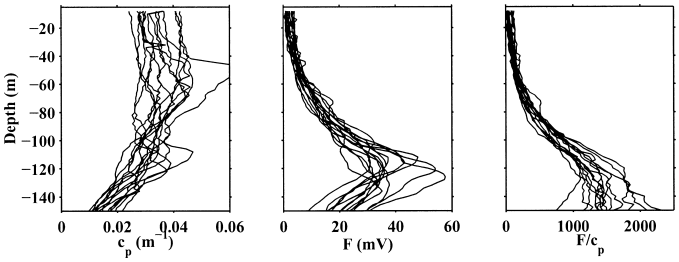

Fig. 6. Profiles of beam attenuation, chlorophyll fluorescence, and the fluorescence to c_p ratio at Sta. ALOHA during stratification (see text for details).

of phytoplankton biomass, chlorophyll, and the chlorophyll : biomass ratio at Sta. ALOHA and in Crater Lake in a systematic way using time-series data from both stations. In Crater Lake, we used bottle determinations of chlorophyll and phytoplankton biovolume and calculated the mean vertical distributions for June 1989–September 2000. At Sta. ALOHA, we used daily mean fluorescence and beam attenuation profiles to estimate POC and chlorophyll concentrations. We calculated daily mean profiles, to minimize the effects of nonphotochemical quenching and internal waves. The chlorophyll and POC concentrations in the upper 120 m of the water column were not correlated, and their ratio varied between 0.002 and 0.02 g Chl (g C)$^{-1}$ (Fig. 5). These values are consistent with Chl : C ratios reported elsewhere for the subtropical North Pacific by Sharp et al. (1980) and Eppley et al. (1988) and Chl : C ratios from laboratory studies. Eppley et al.(1988) found phytoplankton Chl : C ratios of 0.011–0.023 g Chl (g C)$^{-1}$ in the deep chlorophyll maximum, and Sharp et al. (1980) reported values of 0.0025–0.0156 g Chl (g C)$^{-1}$ in the upper 80 m of the euphotic zone. Chl : C ratios reported from laboratory studies vary between 0.0013 and 0.1 g Chl (g C)$^{-1}$ (Falkowski and Owens 1980; Laws and Bannister 1980; Raps et al. 1983; Geider et al. 1985, 1986; Sakshaug et al. 1989).

It is known that the cellular Chl : C ratio in phytoplankton acclimates to changes in irradiance, nutrient availability, and temperature (Falkowski 1980; Laws and Bannister 1980; Cullen 1982; Geider et al. 1987; Sakshaug et al. 1989). Acclimation to changes in irradiance (photoacclimation) has been observed to be rapid (within a few hours) in laboratory studies (Falkowski 1980), which suggests that the pigment metabolism is highly dynamic. In an actively mixed water column, where cells are displaced vertically on time scales smaller than the time it takes to acclimate to the experienced light shift, the response to the cell's recent light history is affected by the mixing regime. The Chl : C characteristics of these rapidly mixed cells will not reflect the current light condition. In this case, there is no large discrepancy between biomass and pigment distribution (Loisel and Morel 1998). We discuss the vertical Chl : C structure only for profiles with a stratified water column and consider the water column as stratified if a density gradient $\Delta\sigma_t > 0.02$ kg m^{-4} occurs at a depth of <50 m.

At Sta. ALOHA, the vertical structures of chlorophyll and particulate matter (Fig. 6) were qualitatively different. The particulate concentrations were at maximum and were relatively constant with depth in the upper 80 m of the water column, slightly decreasing below 100 m. Most of the variation in particulate concentrations (between 1.5 and 3.5 mmol C m^{-3}) occurred between profiles. The chlorophyll concentrations showed little variation between profiles but did show a pronounced increase with depth from ~0.06 mg m^{-3} at the surface to up to 0.3 mg m^{-3} at 120 m in all profiles. The Chl : POC ratio increased exponentially with depth and showed a striking agreement between profiles (Fig. 6).

In Crater Lake, the mean distribution of phytoplankton biovolume has two distinct vertical maxima (Fig. 7). A shallow subsurface maximum is located in the upper 20 m. This shallow maximum is a reoccurring feature in August and is due to subsurface blooms of the diatom *Nitzschia gracilis* (McIntire et al. 1996). A deeper, more pronounced maximum in biovolume is located between 80 and 100 m. The mean vertical chlorophyll profile is qualitatively similar to those at Sta. ALOHA, with low values at the surface and monotonically increasing concentrations at depth to a maximum concentration at ~120 m. The vertical distribution of the chlorophyll to biomass ratio is similar to the Chl : POC profiles at Sta. ALOHA, with monotonically increasing ratios to a maximum at ~120 m depth (Fig. 7).

In summary, these observations show that chlorophyll concentrations in these oligotrophic systems do not represent phytoplankton biomass (in units of carbon), because the ratio of chlorophyll : phytoplankton biomass changes dramatically with depth; phytoplankton grow in the upper part of the euphotic zone, despite the depletion of inorganic nutrients; and, because the maxima of phytoplankton biomass and chlorophyll are separated, the mechanisms for their generation are likely to be different.

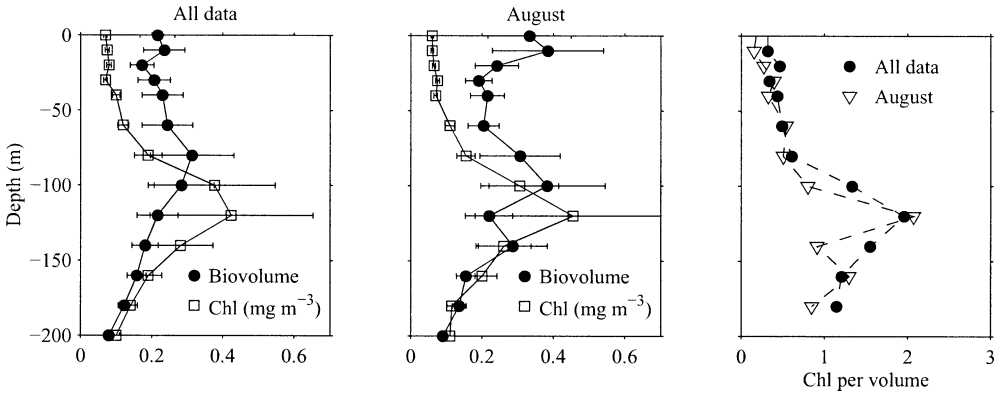

Fig. 7. Mean profiles of chlorophyll and phytoplankton biovolume (mean distributions for all data from 1989 to 2000 and August values only) and mean chlorophyll per phytoplankton volume ratios (for all data and August data only).

Mathematical framework

We formulate a set of general, one-dimensional differential equations for phytoplankton biomass, dissolved nutrients, and chlorophyll and discuss steady-state solutions for nutrient-saturated and -limited growth of phytoplankton. The model is deliberately simple and is based on the fundamental physical and biochemical processes that determine the vertical distribution of phytoplankton biomass and chlorophyll. We use parameterizations of phytoplankton growth and losses, sinking, and vertical diffusion but neglect much of the complexity in natural systems. We consider this simplicity valuable, because only a few ''tunable'' parameters have to be specified. A simple model can elucidate dependencies that are not easily seen in observations and suggest the likely regulating processes. The only spatial dimension in our model is depth, *z*. We neglect horizontal processes, although the vertical distribution of phytoplankton can be affected by such processes (e.g., Franks 1995).

In the case of nutrient-saturated growth, we assume that nutrient supply is sufficient to support optimal growth of phytoplankton. We discuss the effects of a variable sinking/swimming velocity and a vertical mixing structure that includes a surface mixed layer. We then generalize to allow nutrient limitation by including an explicit equation for nutrients. In this case, the phytoplankton growth rate is depressed at nutrient levels below the saturating concentrations. Finally, we include an equation for chlorophyll to allow for photoacclimation.

A simple phytoplankton model with nutrient-saturated growth—The main processes determining the vertical distribution of phytoplankton are growth, biological losses (due to respiration, mortality, and grazing), sinking, and vertical mixing. A general, one-dimensional phytoplankton equation that includes the above processes can be written as

$$\frac{\partial P}{\partial t} + \frac{\partial (w_s P)}{\partial z} = (\mu - R)P + \frac{\partial}{\partial z}\left(k_z \frac{\partial P}{\partial z}\right) \qquad (1)$$

where P is the phytoplankton biomass (in units of carbon or nitrogen), w_s is the settling velocity of phytoplankton, μ is the growth rate, R is the rate of biological losses (including grazing, respiration, and mortality), and k_z is the eddy diffusion coefficient (Riley et al. 1949). w_s, μ, R, and k_z are functions of the depth z and time t. z is defined as increasing toward the sea surface. A comprehensive list of symbols is given in Table 2.

We solved Eq. 1 for steady-state, time-averaged distributions because we want to explain persisting features in the vertical structure of phytoplankton. A system could be assumed to be in steady state if the timescale of adjustment of the system to perturbations is smaller than the timescale at which the system is perturbed. The timescales for adjustment in this problem are on the order of days to a week, as based on dimensional analysis (with the length scale being $1/k_d$, the timescales are $1/[w_s k_d]$, $1/R$, $1/\mu_{\max}$, and $1/[k_z k_d^2]$; *see Table 3*). Thus, steady state is a reasonable assumption for nonbloom conditions in the oligotrophic ocean and in higher latitudes between the spring and the autumn blooms and below the atmospherically forced mixed layer. In the steady-state case, the first term in Eq. (1) can be neglected, and the equation is simplified to the second-order ordinary differential equation (ODE)

$$\frac{d(w_s P)}{dz} = (\mu - R)P + \frac{d}{dz}\left(k_z \frac{dP}{dz}\right) \qquad (2)$$

Equation 2 was derived by Riley et al. (1949), who analyzed it for constant w_s, k_z, and a step function of μ. Steele and Yentsch (1960) analyzed Eq. 2 for variable μ and w_s. Although these two studies did not distinguish between phytoplankton biomass, which is represented by Eq. 2, and chlorophyll concentration, Steele (1964) drew attention to the potential importance of photoacclimation, implying that a maximum in chlorophyll does not necessarily correspond to a maximum in phytoplankton biomass.

Riley et al. (1949) noted that Eq. 2 does not have a nontrivial solution for all sets of parameters. There exist combinations of sinking velocity, growth and loss parameters, and diffusion coefficients, which will yield negative values of phytoplankton concentration and for which no physical solution exists. We refer the reader to Riley et al. (1949),

Table 2. List of symbols.

Notation	
z	Depth
t	Time
P	Phytoplankton concentration
P_0	Phytoplankton boundary condition
N	Nutrient concentration
N_0	Nutrient boundary condition
C	Chlorophyll concentration
μ	Phytoplankton growth rate
$\mu_{\max}$	Maximum phytoplankton growth rate
R	Phytoplankton loss rate (including mortality, respiration, and grazing)
w_s	Phytoplankton sinking velocity
k_N	Half-saturation concentration for nutrient uptake
k_z	Vertical eddy diffusion coefficient
k_d	Diffuse attenuation coefficient of PAR
$z_{\max}$	Depth of phytoplankton maximum
L	Length scale (here, euphotic depth)
$\hat{\alpha}$	Ratio of initial slope of photosynthesis-irradiance curve and maximum rate of photosynthesis ($\hat{\alpha} = \alpha/P^{B}_{\max}$)
$E_{0,\mathrm{PAR}}$	Scalar photosynthetically active radiation
g	Gravitational acceleration
ρ_p	Density of particle
ρ_w	Density of water
R	Radius of particle
η	Kinematic viscosity
Γ	Mixing efficiency
ε	Energy dissipation rate
N^2	Brunt-Väisälä frequency
ρ_{chl}	Fraction of chlorophyll synthesis
Φ	Ratio of chlorophyll to phytoplankton biomass
Φ_m	Maximum ratio of chlorophyll to phytoplankton biomass
α_{chl}	Chlorophyll-specific initial slope of photosynthesis-irradiance curve

who derived the conditions for the existence of a physical solution for a semiconstant growth rate (step function).

Lande et al. (1989) described a method to estimate the net population growth rate—that is, the reproductive rate minus the mortality rate ($\mu - R$), based on Eq. 2. Under the assumption that neutrally buoyant cells ($w_s = 0$), Lande and colleagues estimated the net population growth rate in situ from measurements of vertical distributions of phytoplankton abundance and physical measurements of turbulent diffusion rates as

$$\mu - R = \frac{1}{P}\frac{d}{dz}\left(k_z\frac{dP}{dz}\right)$$

Lande and Wood (1987) estimated the average time a particle remains in the euphotic zone by analyzing stochastic trajectories of individual particles. They showed that the sinking rate of particles within the mixed layer—that is, the region of high turbulent diffusivity—has little effect on the average time particles remain in the mixed layer. However, in the region of low diffusivity below the mixed layer, the sinking rate has a major influence on the average time particles remain in the euphotic zone.

Condition for the existence of a phytoplankton biomass maximum—Examination of Eq. 2 yields a condition for the existence and location of a particle maximum. The condition for a maximum $P(z_{\max})$ (e.g., Steele and Yentsch 1960) is

$$\left.\frac{dP}{dz}\right|_{z_{\max}} = 0 \Rightarrow \left(\mu - R - \frac{dw_s}{dz}\right)P(z_{\max}) + k_z\frac{d^2P(z_{\max})}{dz^2} = 0 \quad (3)$$

and

$$\left.\frac{d^2P}{dz^2}\right|_{z_{\max}} = \frac{1}{k_z}\left(R + \frac{dw_s}{dz} - \mu\right)P(z_{\max}) < 0$$

$$\Rightarrow \left(\mu - R - \frac{dw_s}{dz}\right) > 0 \quad (4a)$$

Table 3. Model parameters. Where parameters do not apply to all numerical examples, references to the respective figures are given.

Symbol	Parameter	Value	Units
$\mu_{\max}$	Nutrient-saturated growth rate (Figs. 8–12)	0.44	d^{-1}
k_N	Half-saturation concentration (Figs. 11, 12)	0.5	mmol N m^{-3}
$\hat{\alpha}$	Ratio of initial slope of P-I curve and maximum rate of photosynthesis (Figs. 8–11)	0.02	$(W\ m^{-2})^{-1}$
α_{chl}	Chlorophyll-specific initial slope of growth versus irradiance curve (Fig. 12)	0.1	mol N (g chl)$^{-1}$ × $(W\ m^{-2})^{-1}$
Φ_m	Maximum chlorophyll to nitrogen ratio (Fig. 12)	2	g chl (mol N)$^{-1}$
R	Loss rate (Figs. 8–12)	0.41	d^{-1}
w_s	Sinking velocity	1	m d^{-1}
k_d	Attenuation of downwelling radiation	0.04*	m^{-1}
k_z	Vertical eddy diffusivity (Figs. 8, 9)	10^{-5}	$m^2\ s^{-1}$
ρ_p	Particle density (Fig. 10)	1,500†	kg m^{-3}
η	Kinematic viscosity (Fig. 10)	0.001	kg $m^{-1}\ s^{-1}$
R	Particle radius (Fig. 10)	10	μm
P_0	Phytoplankton concentration at $z = 0$ (Figs. 8–10)	0.1	mmol N m^{-3}
N_0	Nutrient concentration at $z \to -\infty$ (Fig. 11)	30	mmol N m^{-3}

* Mean value of the observed vertical attenuation (Ricardo Letelier, pers. comm.)
† Value adapted from Lerman et al. (1974).

In regions of low diffusivity, the particle maximum is usually located below the mixed layer. More specifically, this occurs when $k_z \ll w_s L$, where L is the length scale of the problem, (e.g., the euphotic depth). In this case, we can neglect the diffusive flux term in Eq. 3 and obtain

$$\mu - R - \frac{dw_s}{dz} = 0 \tag{4b}$$

at the particle maximum. In other words, at the particle maximum the community growth rate μ equals the sum of the biological losses R (due to respiration and grazing) and the divergence of particles due to changes in the settling velocity. Note that this argument is also valid, with minor changes, if grazing and growth are not proportional to the phytoplankton concentration. Although the second derivative of P is zero in this case, it can be shown that the fourth derivative is negative in most relevant cases and, therefore, that a maximum exists.

For passive particles, the settling/rising velocity is proportional to the difference between the density of the particles and the surrounding water. It follows that a gradient in the settling/rising velocity occurs at pycnoclines—that is, the settling/rising of particles contributes to the condition for an extreme in Eq. (3) only at a pycnocline. However, for realistic density profiles, this contribution is not significant, as we will see in the next subsection (*see also* Steele and Yentsch 1960; Pak et al. 1980). It has been suggested that variations in the settling velocity due to physiological responses of phytoplankton to light or nutrient conditions can contribute to vertical phytoplankton maxima in a significant way (Steele and Yentsch 1960; Bienfang et al. 1983). A divergence in the settling velocity is, however, neither sufficient nor necessary for the existence of a particulate maximum. The balance among all the terms (growth, biological losses, and the divergence in sinking velocity) determines the position of the subsurface particle maximum (Eq. 4b).

The condition for a phytoplankton maximum (Eqs. 3 and 4) is general and also applies if we assume a community comprised of phytoplankton cells with different growth, loss, and sinking characteristics. If we assume that each of a number of j different groups of phytoplankton obey

$$\frac{d(w_{sj}P_j)}{dz} = (\mu_j - R_j)P_j + \frac{d}{dz}\left(k_z \frac{dP_j}{dz}\right),$$

summation of the j equations and definition of the community growth, loss, and settling rates as

$$w_s \equiv \frac{1}{P}\sum_j w_{sj}P_j, \qquad \mu \equiv \frac{1}{P}\sum_j \mu_j P_j, \text{ and}$$

$$R \equiv \frac{1}{P}\sum_j R_j P_j$$

where $P = \Sigma_j P_j$ yields Eq. 2.

Process parameterizations—For illustrative purposes, we define parameterizations of growth, biological losses, sinking, and vertical diffusion, which allow us to discuss numerical solutions of Eq. 2. The growth rate is assumed to follow

$$\mu = \mu_{\max}[1 - \exp(-\hat{\alpha}\, E_{0,\mathrm{PAR}})]$$

where $\mu_{\max}$ is the nutrient-saturated phytoplankton growth rate, $E_{0,\mathrm{PAR}}$ is the scalar photosynthetically active irradiance, and $\hat{\alpha}$ is the ratio of the initial slope of the photosynthesis-irradiance curve (usually denoted as α) and the maximum rate of photosynthesis (often denoted as $P^B_{\max}$). The scalar irradiance as function of depth is parameterized by

$$E_{0,\mathrm{PAR}}(z) = E_{0,\mathrm{PAR}}(z = 0)\exp(k_d z)$$

with k_d as the diffuse attenuation coefficient of the photosynthetically available radiation (PAR). This formulation neglects the change in attenuation for the different spectral components of the downwelling light (Morel 1988). For the sake of simplicity, we also ignore the effects of the dissolved and particulate material on the attenuation coefficient k_d.

Because phytoplankton respiration and grazing rates are poorly constrained parameters and are hard to separate in field measurements, we assume R to be constant with depth for the numerical solutions presented in the present article.

For low Reynolds numbers (Re $\ll$ 1), the sinking of particles is described by the Stokes' law (Gibbs et al. 1971). The settling velocity of a spherical particle can be parameterized by

$$w_s = 2g\frac{\rho_P - \rho_w}{9\eta}r^2 \tag{5}$$

where g is the gravitational acceleration; ρ_p and ρ_w are the densities of the particle and the surrounding water, respectively; η is the kinematic viscosity; and r is the particle radius (Lerman et al. 1974). For spherical particles, the Reynolds numbers are low in the size range 0.3–30 μm in radius. The settling velocity depends primarily on the density and size of the settling particles and also on the viscosity of the surrounding water, which is a function of temperature, and on the particle shape. The density of algal cells varies depending on their physiological status, and active buoyancy regulation has been observed (e.g., Villareal et al. 1993). Richardson and Cullen (1995) reported near-neutral density in a culture of the diatom *Thalassiosira weissflogii* under nutrient-replete conditions and an increasing cell density and sinking rate subsequent to nutrient depletion. Contradicting evidence about the connection between nutritional status and sinking rates has been found in natural populations that include various types of phytoplankton (e.g., Bienfang and Harrison 1984), which suggests that not all phytoplankton respond to nutrient depletion in the same way. For the present study, we do not attempt to parameterize the effect of physiological changes in cell density on sinking rates but consider idealized cases of vertically varying sinking velocities.

We parameterized the eddy diffusivity using the Brunt-Väisälä frequency N^2, suggested by Gargett (1984) and Gregg et al. (1986), as

$$k_z = \frac{\Gamma\varepsilon}{N^2}, \quad \text{where} \quad N^2 = \frac{-g}{\rho_w}\frac{d\rho_w}{dz} \tag{6}$$

where Γ is the mixing efficiency, ε is the energy dissipation rate, g is the gravitational acceleration, and ρ_w is the water

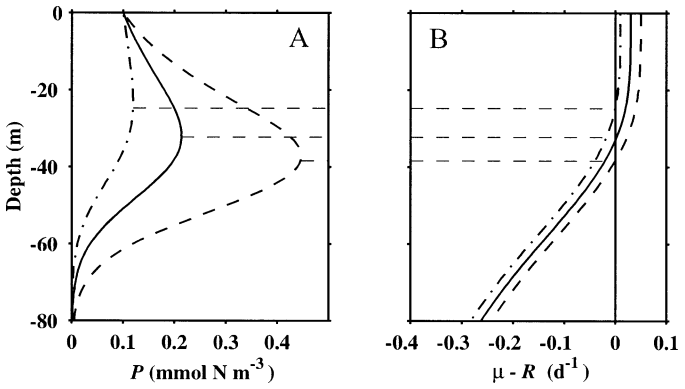

Fig. 8. Profiles of (A) phytoplankton P for a constant settling velocity and (B) growth minus losses. Variations in the phytoplankton loss rate lead to variations in the phytoplankton maximum, because its location occurs where $\mu - R = 0$ (the dashed curve corresponds to $R = 0.39$ d^{-1} and the dash-dotted curve to $R = 0.43$ d^{-1}).

density. Gregg et al. (1986) estimated a mean value of $\Gamma\varepsilon$ at the thermocline to be 3.7×10^{-10} W kg^{-1}.

Numerical solutions for nutrient-saturated growth—To solve Eq. 2, which is a second-order ODE, two boundary conditions need to be specified. We set $P = P_0$ at the surface and $P \to 0$ for $z \to -\infty$. The specification of the phytoplankton concentration P_0 at the surface might appear as a constraint to the solution, but this boundary condition is necessary to specify one of an infinite number of solutions. Note that every distribution $\hat{P} := c \times P$ where c is an arbitrary constant solves Eq. 2 if P is a solution. We solved the boundary value problem using the two-point boundary value routine in MATLAB. The model coefficients were chosen to represent the system at Sta. ALOHA and are given in Table 3.

Solutions for a vertically constant sinking velocity and a vertically constant diffusivity, but different loss rates R, are shown in Fig. 8. Each solution displays a subsurface maximum at the depth where the growth rate μ equals the losses R as predicted by Eq. 4a,b. For nutrient-saturated conditions, the growth rate of phytoplankton is monotonically decreasing with depth (we assume that no inhibition of growth occurs near the surface). Hence, growth exceeds the losses above the particulate maximum and losses exceed growth below (for negligible divergence in the settling velocity). This suggests that the loss by community respiration and grazing can be estimated if the phytoplankton growth rate and the location of the phytoplankton maximum are known and no vertical variations in sinking velocity occur.

We illustrate the effect of a vertically variable sinking velocity in Fig. 9. If the settling velocity w_s is calculated on the basis of a realistic density profile and constant particle density using the parameterization in Eq. 5, the resulting divergence in settling velocity is small. The density profile (with a density jump from 1,020 to 1,028 kg m^{-3} at 50 m depth) leads to a decrease in settling velocity by $<2\%$. This has virtually no effect on the particle distribution and the location of the particle maximum (compare the solid lines in Figs. 8 and 9, which represent the constant sinking velocity and the sinking velocity based on Eq. 5, respectively). This is in line with dimensional arguments presented by Steele and Yentsch (1960) and Pak et al. (1980) that Stokes' settling in connection with realistic density gradients does not produce a significant divergence in sinking rate. On the other hand, Steele and Yentsch (1960) and Bienfang et al. (1983) provided experimental evidence that settling rates decrease because of physiological responses at low light levels in two diatom species. They found that settling rates were reduced by a factor of two at light levels corresponding to the base of the euphotic zone. Richardson and Cullen (1995) observed, in their experiments, an increase in settling rates of a diatom on nutrient depletion that was probably due to the production of ''ballast'' carbohydrates in the cells. In model calculations, they showed that a ballast-related change of sinking rate by 1.1 m d^{-1} could be explained by the change in carbohydrate to protein ratios inferred from their batch cultures. We constructed profiles of settling rates that decrease from 1.5 to 0.5 m d^{-1} at 30 and 70 m depth, respectively, and calculated the resulting particle distributions

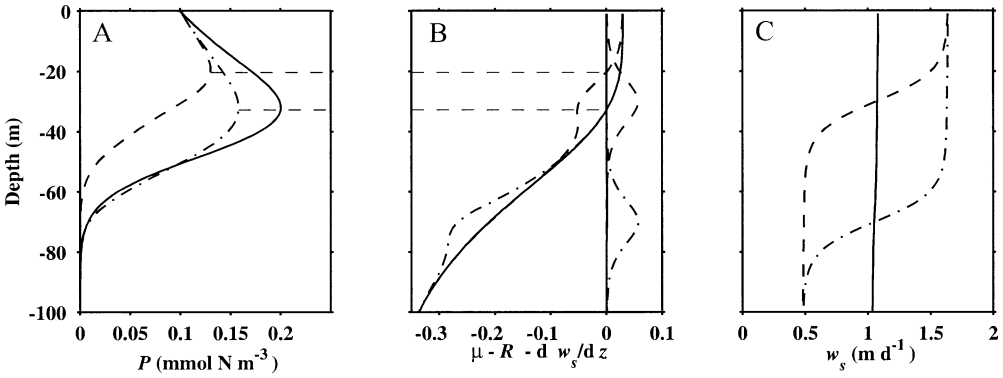

Fig. 9. Profiles of (A) phytoplankton concentration P for different settling velocities w_s, (B) growth minus losses and divergence in settling velocity, and (C) settling velocities. Solid lines represent the case where the settling velocity is based on Stokes' law and a realistic density profile. The dashed and dash-dotted lines correspond to hypothetical settling profiles with a strong gradient at 30 and 70 m depth, respectively.

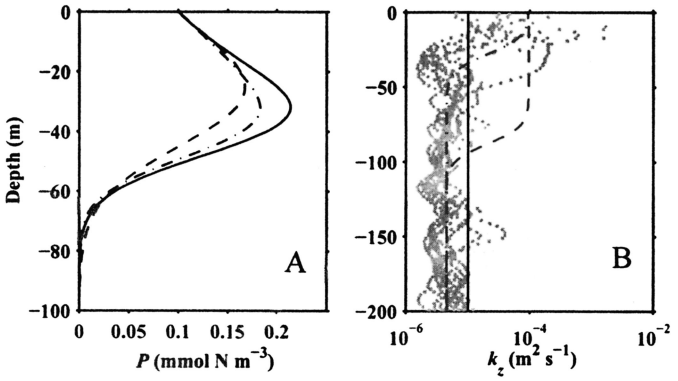

Fig. 10. (A) Particle distributions for (B) different profiles of vertical eddy diffusivity. The solid line represents the vertically constant diffusivity profile and the dashed and dash-dotted lines represent two vertically varying diffusivity profiles. Data-based estimates of the eddy diffusivity (shown as filled gray circles in panel B) are based on the Brunt-Väisälä frequency N^2 (see text for details).

(Fig. 9). In this case, the divergence of the sinking rate contributes to the condition for the particle maximum (Eq. 3) in a significant way but only if it is located above the compensation depth (the depth where $\mu = R$). In general, we do not expect a significant divergence in settling velocity in oligotrophic environments. Phytoplankton there are dominated by small, slow-sinking organisms of <3 μm (e.g., Bienfang et al. 1983), and, as argued by Steele (1964), sinking appears to be an inefficient strategy for phytoplankton under these stable, nutrient-limited conditions. Note that neither stratification nor a divergence in the settling velocity is necessary for the existence of a particle maximum. In addition, we note that the prediction that $\mu = R$ at the phytoplankton maximum can be tested in the environment (e.g., with primary production and grazing dilution experiments).

So far, all calculations have assumed a vertically constant diffusivity. We can generalize our calculations by including a vertically variable profile of eddy diffusivity. This allows us to simulate a surface mixed layer and to demonstrate how the eddy diffusivity contributes to the location of the particle maximum (second term in Eq. 3). On the basis of Eq. 6 and profiles of the Brunt-Väisälä frequency from Sta. ALOHA (13 casts; 17 February 1993), we estimated vertical eddy diffusivities k_z and constructed two profiles of k_z with a surface mixed layer of 20 and 80 m, respectively (Fig. 10B). The resulting particle distributions (Fig. 10A) show that even strong gradients in k_z do not affect the location of the particle maximum if it is located above the compensation depth (dash-dotted line). Only if the mixed layer extends below the compensation depth does mixing become an important term in Eqs. 2 and 3 and is the location of the particle maximum shifted (dashed line).

A simple phytoplankton-nutrient model—Thus far, we have assumed that nutrient levels are sufficient to support nutrient-saturated growth of phytoplankton. However, in the oligotrophic ocean, inorganic nutrient levels are low in the euphotic zone, and the particle maximum is usually located in the low nutrient zone above the nutricline. Therefore, we generalize our model to allow nutrient limitation by including the nutrient N as an additional state variable. N represents the dissolved form of the model's nutrient currency available to phytoplankton (N includes the bioavailable organic and inorganic forms). The steady-state nutrient conservation equation is written as

$$0 = (R - \mu)P + \frac{d}{dz}\left(k_z \frac{dN}{dz}\right) \tag{7}$$

The nutrient and phytoplankton Eqs. 2 and 7 are coupled through the phytoplankton growth rate

$$\mu = \mu_{\max}[1 - \exp(-\hat{\alpha}E_{0,\mathrm{PAR}})]\frac{N}{k_N + N}$$

where k_N is the half-saturation coefficient for nutrient uptake. To solve the two second-order ODEs, Eqs. 2 and 6, numerically, four boundary conditions have to be specified. We can simplify the system by the following consideration. At steady state, the downward flux of particulate material at any given depth has to be balanced by an upward flux of the dissolved nutrient—that is

$$w_s P - k_z \frac{dP}{dz} = k_z \frac{dN}{dz} \tag{8}$$

This condition can simply be derived by adding Eqs. 2 and 6 and integrating vertically with the provision that the flux approaches zero at infinite depth.

Now the problem is simplified to solving the system of the coupled ODEs, Eqs. 2 and 8, and the specification of only three boundary conditions. Like in the case of nutrient-saturated growth, the phytoplankton concentration should approach zero at infinite depth, $P \to 0$ for $z \to -\infty$. We also impose a no-flux condition for nutrients and phytoplankton at the surface. For phytoplankton this is written as $w_s - k_z(dP/dz) = 0$ at $z = 0$. The no-flux condition for phytoplankton implies no-flux for the nutrient, $dN/dz(z = 0) = 0$ (following from Eq. 8). As the third boundary condition, we pose that the nutrient concentration at depth is specified—that is, $N \to N_0$ for $z \to -\infty$. We prefer the specification of a deep nutrient concentration N_0 over the specification of a surface phytoplankton concentration P_0, which was necessary in the case of nutrient-saturated growth, because, for application to real systems, information about the deep nutrient concentrations will be more readily available. An implication of Eq. 8 is that the sum of N and P will increase monotonically below the surface until it equals N_0 at depth, because $d(N + P)/dz = (w_s/k_z)P < 0$ for the positive definite P and k_z and sinking cells ($w_s < 0$). Note that the opposite is true when the cells are buoyant ($w_s > 0$).

A numerical solution for this case is shown in Fig. 11 in comparison with mean profiles of particulate organic nitrogen (PON), nitrate, and total dissolved nitrogen (TDN) from Sta. ALOHA. A maximum of phytoplankton P is predicted similar to the case with nutrient-saturated growth (compare Figs. 8–10). The simulated nutrient N is low at the surface and increases rapidly at the location of the maximum phytoplankton concentration until the deep nutrient concentration N_0 is reached (Fig. 11). Although the simulated and

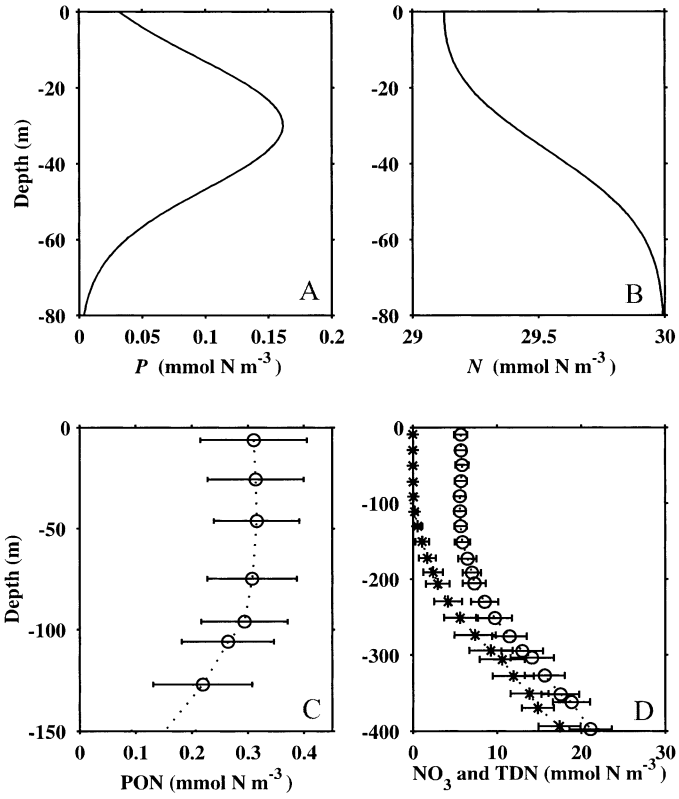

Fig. 11. (A, B) Model-predicted phytoplankton and nutrient profiles in comparison with (C, D) mean observations at Sta. ALOHA. Asterisks in panel D show mean nitrate concentrations, and open circles represent mean TDN.

observed mean profiles agree qualitatively, there are differences that we attribute to the simplicity of our model. The observed mean PON profile displays constant values at the surface and decreases monotonically below 100 m, whereas our simulated phytoplankton *P* shows a pronounced subsurface maximum. The shape of the simulated and observed nutrient profiles differs mainly in steepness, thickness, and location of the nutricline. These discrepancies are not surprising, considering that we assume a single phytoplankton group and neglect the microbial loop and the dynamics of the dissolved organic matter and detritus pools.

Chl a *equation*—The relationship between chlorophyll and phytoplankton biomass (in units of nitrogen or carbon) is nonlinear and nonmonotonic (e.g., Fig. 5), because the ratio of chlorophyll to phytoplankton carbon or nitrogen is variable. Changes in chlorophyll content per cell are due to a physiological response of the photosynthetic apparatus to changes in the light level as well as to nutrient conditions and temperature (Falkowski 1980; Laws and Bannister 1980; Sakshaug et al. 1989). In stable environments, this process determines the vertical chlorophyll profile (Figs. 6 and 7; Pak et al. 1988; Kitchen and Zaneveld 1990). To determine the vertical chlorophyll distribution in our model framework, we include the chlorophyll concentration as an additional state variable (Taylor et al. 1997). The effects of photoacclimation are calculated based on the model of Geider et al. (1996, 1997). The steady-state conservation equation for chlorophyll, *C*, is formulated as

$$\frac{d(w_s C)}{dz} = (\rho_{\text{chl}}\mu - R)C + \frac{d}{dz}\left(k_z \frac{dC}{dz}\right) \tag{9}$$

where ρ_{chl} represents the fraction of phytoplankton growth devoted to chlorophyll synthesis. Following the method of Geider et al. (1997), ρ_{chl} is defined as

$$\rho_{\text{chl}} = \Phi_m \left(\frac{\mu P}{\alpha_{\text{chl}} E_{0,\text{PAR}} C}\right) \tag{10}$$

where Φ_m is the maximum ratio of chlorophyll to phytoplankton biomass, *P*, in units of carbon or nitrogen, and α_{chl} is the chlorophyll-specific initial slope of the photosynthesis irradiance curve. ρ_{chl} is regulated by the ratio of achieved-to-maximum potential photosynthesis $(\mu P)/(\alpha_{\text{chl}} E_{0,\text{PAR}} C)$ (Geider et al. 1997). The phytoplankton growth rate, μ, is determined by

$$\mu = \mu_m \left[1 - \exp\left(\frac{-\alpha_{\text{chl}} E_{0,\text{PAR}} C}{\mu_m P}\right)\right] \tag{11}$$

with

$$\mu_m = \mu_{\max} \frac{N}{k_N + N}$$

For our purposes, we omit the temperature dependence of μ_m that is incorporated in the formulations of Geider et al. (1997) and Taylor et al. (1997). Note that our steady-state equations for phytoplankton biomass, *P*, and chlorophyll, *C* (Eqs. 2 and 9) are coupled through the dependencies in ρ_{chl} and μ.

The numerical solution of Eq. (9) requires the specification of two additional boundary conditions. Analogous to the boundary conditions for phytoplankton, the chlorophyll concentration should approach zero at infinite depth, $C \to 0$ for $z \to -\infty$, and there will be no flux of chlorophyll across the surface—that is, $w_s C + dC/dz = 0$ for $z = 0$. The resulting chlorophyll profiles are shown in Fig. 12. The maxima of phytoplankton and chlorophyll are vertically separated by ~50 m. The vertical structure and the magnitude of the phytoplankton and chlorophyll concentrations agree with the observations from Sta. ALOHA (Fig. 6). The simulated ratios of 0.012–0.025 g Chl (g C)$^{-1}$ in the deep chlorophyll maximum and 0.0038 g Chl (g C)$^{-1}$ at the surface compare well with the ratios observed in the North Pacific subtropical gyre of 0.011–0.023 g Chl (g C)$^{-1}$ at the deep chlorophyll maximum (Eppley et al. 1988) and 0.0025–0.0156 g Chl (g C)$^{-1}$ for the upper 80 m (Sharp et al. 1980).

The steady-state export flux of particulate matter in this simulation is 0.2 mmol N m^{-2} d^{-1} at 100 m depth (Fig. 12). For comparison, the mean export flux observed at Sta. ALOHA was 28.3 ± 9.91 mg C m^{-2} d^{-1} (11-year mean; Karl et al. 2001), which corresponds to 0.356 ± 0.125 mmol N m^{-3} d^{-1} (under the assumption of a C : N ratio of 106 : 16).

Discussion

We present a simple mathematical framework to describe the vertical structure of phytoplankton biomass, nutrients,

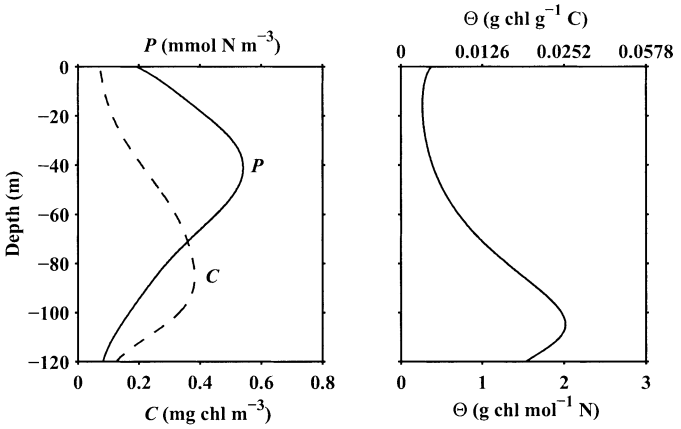

Fig. 12. Model-predicted profiles of phytoplankton *P*, chlorophyll *C*, and the chlorophyll : phytoplankton nitrogen ratio Φ. To compare the simulated values of the chlorophyll : biomass ratio Φ (g Chl mol^{-1} N) with observed ratios, we converted Φ to g Chl (g $C)^{-1}$ by dividing by the Redfield ratio C : N = 106 : 16 and by the molar weight of carbon (upper axis in right panel).

and chlorophyll. The model includes phytoplankton growth, respiratory and grazing losses, sinking/rising, vertical mixing, and photoacclimation and allows one to explore which processes contribute to the generation of vertical maxima. Elements of our model were present already in the models of Riley et al. (1949), Steele and Yentsch (1960), and Steele (1964).

Our model suggests that maxima in phytoplankton biomass exist at the ''general compensation depth,'' where the growth rate is balanced by losses due to respiration and grazing and the divergence in sinking velocity, provided that the vertical diffusivity is small. According to Stokes' Law, a divergence in sinking velocity could be introduced by a change in water density, but density changes at pycnoclines in natural environments are too small to contribute to the above balance in a significant way. Changes in settling velocity have been observed as physiological response to variations in environmental conditions, for example, in light or nutrient levels (Steele and Yentsch 1960; Bienfang et al. 1983; Richardson and Cullen 1995), and the resulting divergence in settling velocity can be large enough to affect the location of the phytoplankton particle maximum. However, in stable, oligotrophic environments with a predominance of small cells, we do not expect a significant contribution from the settling velocity and suggest that, in these environments, the biomass maximum is located at the depth where growth and losses compensate. This is a testable hypothesis.

It has been observed that distinct assemblages of phytoplankton coexist in a given water column in oligotrophic systems (Venrick 1982; McIntire et al. 1996; Moore and Chisholm 1999). Our model suggests a quantitative criterion: a species occurs in highest abundance in the vertical where its species-specific growth and loss rates balance. This is consistent with the findings of Moore and Chisholm (1999), who have shown that different *Prochlorococcus* isolates are photophysiologically adapted to low or high light conditions, resulting in different relative distributions in the water column.

Vertical maxima of phytoplankton biomass (in units of carbon) and chlorophyll are often separated (Steele 1964; Kiefer et al. 1976; Pak et al. 1988; Kitchen and Zaneveld 1990). We provided additional observational evidence for the vertical separation of the phytoplankton biomass maximum and the deep chlorophyll maximum from two oligotrophic systems (Sta. ALOHA in the subtropical North Pacific and Sta. 13 in Crater Lake). In both systems during stable, stratified conditions, phytoplankton biomass is at its maximum concentration in the nutrient-depleted upper 80 m of the water column, well above the chlorophyll maximum located at ~120 m. This separation implies an increase in the chlorophyll to biomass ratio with depth, which can be attributed mainly to photoacclimation, although higher nutrient concentrations at depth can also play a role.

Results from laboratory experiments (Geider et al. 1987; Kana and Glibert 1987) and observations from stable, oligotrophic environments (e.g., Kitchen and Zaneveld 1990) suggest that the response of the algal chlorophyll to carbon ratio can be predicted reasonably well and is inversely related to mean irradiance (Steele 1964; Kiefer and Kremer 1981; Geider et al. 1997). The inclusion of the photoacclimation model of Geider et al. (1997) in our model framework predicted a vertical separation of the phytoplankton biomass and chlorophyll maximum by 50 m, monotonically increasing chlorophyll concentrations that agree well with observed profiles, and chlorophyll to carbon ratios in agreement with observed values from the subtropical North Pacific.

Our model simplifies the functioning of the pelagic ecosystem and its temporal and spatial representation, under the assumption that the system is strictly vertical and in steady state. We only consider one group of ''average'' phytoplankton, neglect food-web and microbial loop dynamics (detritus, dissolved organic matter, and zooplankton are not included explicitly), and assume the respirative and grazing losses of phytoplankton to be constant with depth. The vertical swimming of phytoplankton is also neglected (its average effect can be lumped into the ''eddy'' diffusivity). Although these simplifications certainly hinder a quantitative comparison of model results and observations, they allow the investigation of how basic processes contribute to the vertical structure of phytoplankton biomass and chlorophyll in general. The assumption of steady state will be violated during episodic events of strong physical forcing, nutrient injection, or blooms. The assumption of strictly vertical fluxes will not adequately represent coastal environments. Our model also neglects some feedback mechanisms, like the effect of biomass on light attenuation. Although these are important aspects that could be included, their addition is unlikely to change our conclusions qualitatively.

Chlorophyll is the most widely used index of phytoplankton abundance and productivity in the ocean, mainly because fluorometry and satellite imagery allow efficient observations with high spatial and temporal coverage. Direct measurements of organic carbon or organic nitrogen, which are ecologically more relevant units of phytoplankton biomass (e.g., Cullen 1982), are much more complicated. Although

the relationship between the chlorophyll pigment concentration and phytoplankton carbon content or productivity is highly variable, it is accepted as a ''pragmatic surrogate'' (Falkowski and Raven 1997) and is used in models of primary productivity (Behrenfeld and Falkowski 1997) and for data assimilation in ecological models (Friedrichs 2002; Natvik and Evensen 2003). The plasticity in cellular chlorophyll quotas impedes a simple conversion from chlorophyll to biomass and a mechanistic description of these variations, and their inclusion in primary productivity and ecological models is needed. We see real potential in using optically derived measures of particle concentration like beam attenuation. For example, productivity estimates could be improved using measures of phytoplankton carbon derived from space and could be assimilated into ecosystem models to constrain model parameters.

References

BEERS, J. R., F. M. H. REID, AND G. L. STEWART. 1975. Microplankton of the North Pacific Central Gyre. Population structure and abundance in, June 1973. Int. Rev. Gesam. Hydrobiol. **60:** 607–638.

BEHRENFELD, M. J., AND P. G. FALKOWSKI. 1997. A consumer's guide to phytoplankton primary productivity models. Limnol. Oceanogr. **42:** 1479–1491.

BIENFANG, P. K., AND P. J. HARRISON. 1984. Sinking-rate response of natural assemblages of temperate and subtropical phytoplankton to nutrient depletion. Mar. Biol. **83:** 293–300.

———, J. SZYPER, AND E. LAWS. 1983. Sinking rate and pigment responses to light-limitation in a marine diatom: Implications to dynamics of chlorophyll maximum layers. Oceanol. Acta **6:** 55–62.

BISHOP, J. K. B. 1999. Transmissometer measurement of POC. Deep-Sea Res. I **46:** 353–369.

———, S. E. CALVERT, AND M. Y. S. SOON. 1999. Spatial and temporal variability of POC in the northeast Subarctic Pacific. Deep-Sea Research II **46:** 2699–2733.

BOSS, E., AND OTHERS. 2001. The spectral particulate attenuation and particle size distribution in the bottom boundary layer of a continental shelf. J. Geophys. Res. **106:** 9499–9508.

CHANG, G. C., AND T. D. DICKEY. 2001. Optical and physical variability on time scales from minutes to the seasonal cycle on the New England shelf: July 1996–June 1997. J. Geophys. Res. **106:** 9435–9453.

CULLEN, J. J. 1982. The deep chlorophyll maximum: Comparing vertical profiles of chlorophyll. Can. J. Fish. Aquat. Sci. **39:** 791–803.

———, AND R. W. EPPLEY. 1981. Chlorophyll maximum layers of the Southern California Bight and possible mechanisms of their formation and maintenance. Oceanol. Acta **4:** 23–32.

DAVIS, R. F., C. C. MOORE, J. R. V. ZANEVELD, AND J. M. NAPP. 1997. Reducing the effects of fouling on chlorophyll estimates derived from long-term deployments of optical instruments. J. Geophys. Res. **102:** 5851–5855.

DURAND, M. D., R. J. OLSON, AND S. W. CHISHOLM. 2001. Phytoplankton population dynamics at the Bermuda Atlantic Time-series station in the Sargasso Sea. Deep-Sea Res. II **48:** 1983–2003.

EPPLEY, R. W., E. SWIFT, D. G. REDALJE, M. R. LANDRY, AND L. W. HASS. 1988. Subsurface chlorophyll maximum in August–September 1985 in the CLIMAX area of the North Pacific. Mar. Ecol. Prog. Ser. **42:** 289–301.

FALKOWSKI, P. G. 1980. Light-shade adaptation n marine phytoplankton, p. 99–119. *In* P. G. Falkowski [ed.], Primary productivity in the sea. Plenum.

———, AND T. G. OWENS. 1980. Light-shade adaptation. Plant Physiol. **66:** 592–595.

———, AND J. A. RAVEN. 1997. Aquatic photosynthesis. Blackwell Science.

FRANKS, P. J. S. 1995. Thin layers of phytoplankton: A model of formation by near inertial wave-shear. Deep-Sea Res. I **42:** 75–91.

FRIEDRICHS, M. A. M. 2002. Assimilation of JGOFS EqPac and SeaWiFS data into a marine ecosystem model of the central equatorial Pacific Ocean. Deep-Sea Res. II **49:** 289–320.

GARDNER, W. D., M. S. RICHARDSON, AND W. O. SMITH. 2000. Seasonal patterns of water column particulate organic carbon and fluxes in the Ross Sea, Antarctica. Deep-Sea Res. II **47:** 3423–3449.

GARGETT, A. E. 1984. Vertical eddy diffusivity in the ocean interior. J. Mar. Res. **42:** 359–393.

GEIDER, R. J., H. L. MCINTYRE, AND T. M. KANA. 1996. A dynamic model of photoadaptation in phytoplankton. Limnol. Oceanogr. **41:** 1–15.

———, ———, AND ———. 1997. Dynamic model of phytoplankton growth and acclimation: Responses of the balanced growth rate and the chlorophyll *a*:carbon ratio to light, nutrient-limitation and temperature. Mar. Ecol. Prog. Ser. **148:** 187–200.

———, B. A. OSBORNE, AND J. A. RAVEN. 1985. Light effects on growth and photosynthesis in *Phaeodactylum tricornutum* (Bacillariophyceae). J. Phycol. **21:** 609–619.

———, ———, AND ———. 1986. Growth, photosynthesis and maintenance metabolic cost in the diatom *Phaeodactylum tricornutum* at very low light levels. J. Phycol. **22:** 39–48.

———, ———, AND ———. 1987. Light and temperature dependence of the carbon to chlorophyll a ratio in microalgae and cyanobacteria: Implications for physiology and growth of phytoplankton. New Phytol. **106:** 1–34.

GIBBS, R. J. 1979. Chlorophyll *b* interference in the fluorometric determination of chlorophyll *a* and phaeo-pigments. Aust. J. Mar. Freshw. Res. **30:** 597–606.

———, M. D. MATTHEWS, AND D. A. LINK. 1971. The relationship between sphere size and settling velocity. J. Sediment. Petrol. **41:** 7–18.

GREGG, M. C., E. A. D'ASARO, T. J. SHAY, AND N. LARSON. 1986. Observations of persistent mixing and near-inertial internal waves. J. Phys. Oceanogr. **16:** 856–885.

GUNDERSON, J. S., W. D. GARDNER, M. J. RICHARDSON, AND I. D. WALSH. 1998. Effects of monsoons on the seasonal and spatial distribution of POC and chlorophyll in the Arabian Sea. Deep-Sea Research II **45:** 2103–2132.

JUMARS, P. A. 1993. Concepts in biological oceanography. Oxford Univ. Press.

KANA, T. M., AND P. M. GLIBERT. 1987). Effect of irradiance up to 2000 μE m^{-2} s^{-1} on marine *Synechococcus* WH7803-I. Growth pigmentation, and cell composition. Deep-Sea Res. **34:** 479–495.

KARL, D. M., J. E. DORE, R. LUKAS, A. F. MICHAELS, N. R. BATES, AND A. KNAP. 2001. Building the long-term picture: The U.S. JGOFS time-series programs. Oceanography **14:** 6–17.

KIEFER, D. A., AND J. N. KREMER. 1981. Origins of the vertical patterns of phytoplankton and nutrients in the temperate, open ocean: A straitgraphic hypothesis. Deep-Sea Res. **28:** 1087–1105.

———, R. J. OLSON, AND O. HOLM-HANSEN. 1976. Another look at the nitrite and chlorophyll maxima in the central North Pacific. Deep-Sea Res. **23:** 1199–1208.

KITCHEN, J. C., AND J. R. ZANEVELD. 1990. On the noncorrelation

of the vertical structure of light scattering and chlorophyll a in case I waters. J. Geophys. Res. **95:** 20237–20246.

LANDE, R., AND A. M. WOOD. 1987. Suspension times of particles in the upper ocean. Deep-Sea Res. **34:** 61–72.

LANDE, R., W. K. W. LI, E. P. W. HORNE, AND A. M. WOOD. 1989. Phytoplankton growth rates estimated from depth profiles of cell concentration and turbulent diffusion. Deep-Sea Res. **36:** 1141–1159.

LARSON, G. L., C. D. MCINTIRE, M. HURLEY, AND M. W. BUKTENICA. 1996. Temperature, water chemistry, and optical properties of Crater Lake. Lake Reservoir Manag. **12:** 230–247.

LAWS, E. A. 1997. Mathematical methods for oceanographers. Wiley.

———, AND T. T. BANNISTER. 1980. Nutrient- and light-limited growth of *Thalassiosira fluviatilis* in continuous culture, with implications for phytoplankton growth in the ocean. Limnol. Oceanogr. **25:** 457–473.

LERMAN, A., D. LAL, AND M. F. DACEY. 1974. Stokes settling and chemical reactivity of suspended particles in natural waters, p. 17–47. *In* R. J. Gibbs [ed.], Suspended solids in water. Plenum.

LETELIER, R. M., J. E. DORE, C. D. WINN, AND D. M. KARL. 1996. Seasonal and interannual variations in photosynthetic carbon assimilation at station ALOHA. Deep-Sea Res. II **43:** 467–490.

LOISEL, H., AND A. MOREL. 1998. Light scattering and chlorophyll concentration in case 1 waters: A reexamination. Limnol. Oceanogr. **43:** 847–858.

MANN, K. H., AND J. R. N. LAZIER. 1996. Dynamics of marine ecosystems. Blackwell Science.

MCINTIRE, C. D., G. L. LARSON, R. E. TRUITT, AND M. K. DEBACON. 1996. Taxonomic structure and productivity of phytoplankton assemblages in Crater Lake, Oregon. Lake Reservoir Manag. **12:** 259–280.

MOORE, L., AND S. W. CHISHOLM. 1999. Photophysiology of the marine cyanobacterium Prochlorococcus: Ecotypic differences among cultured isolates. Limnol. Oceanogr. **44:** 628–638.

MOREL, A. 1973. Diffusion de la lumiere par les eaux de mer. Resultats experimentaux et approche theorique. Optics of the sea. AGARD Lect. Ser. **61:** 31.1–31.76.

———. 1988. Optical modeling of the upper ocean in relation to its biogenous matter content (case I waters). J. Geophys. Res. **93:** 10749–10768.

MORROW, J. H., W. S. CHAMBERLIN, AND D. A. KIEFER. 1989. A two-component description of spectral absorption by marine particles. Limnol. Oceanogr. **34:** 1500–1509.

NATVIK, L. J., AND G. EVENSEN. 2003. Assimilation of ocean color data into a biochemical model of the North Atlantic: Part I Data assimilation experiments. J. Mar. Syst. **40–41:** 127–153.

PAK, H., D. A. KIEFER, AND J. C. KITCHEN. 1988. Meridional variations in the concentration of chlorophyll and microparticles in the North Pacific Ocean. Deep-Sea Res. I **35:** 1151–1171.

———, R. V. ZANEVELD, AND J. C. KITCHEN. 1980. Intermediate nephleoid layers observed off Oregon and Washington. J. Geophys. Res. **85:** 6697–6708.

RAPS, S., K. WYMAN, H. W. SIEGELMAN, AND P. G. FALKOWSKI. 1983. Adaptation of the cyanobacterium *Microcystis aeruginosa* to light intensity. Plant Physiol. **72:** 829–832.

RICHARDSON, T. L., AND J. J. CULLEN. 1995). Changes in buoyancy and chemical composition during growth of a coastal marine diatom: Ecological and biogeochemical consequences. Mar. Ecol. Progr. Ser. **128:** 77–90.

RILEY, G. A., H. STOMMEL, AND D. F. BUMPUS. 1949. Quantitative ecology of the plankton of the western North Atlantic. Bull. Bingham Oceanogr. Coll. **12:** 1–169.

ROESLER, C. S., M. J. PERRY, AND K. L. CARDER. 1989. Modeling in situ phytoplankton absorption from total absorption spectra in productive inland marine waters. Limnol. Oceanogr. **34:** 1510–1523.

SAKSHAUG, E., K. ANDRESEN, AND D. A. KIEFER. 1989. A steady state description of growth and light absorption in the marine planktonic diatom *Skeletonema costatum.* Limnol. Oceanogr. **34:** 198–205.

SHARP, J. H., M. J. PERRY, E. H. RENGER, AND R. W. EPPLEY. 1980. Phytoplankton rate processes in the oligotrophic waters of the central North Pacific Ocean. J. Plankton Res. **2:** 335–353.

STEELE, J. 1964. A study of production in the Gulf of Mexico. J. Mar. Res. **3:** 211–222.

———, AND C. S. YENTSCH. 1960. The vertical distribution of chlorophyll. J. Mar. Biol. Assoc. U.K. **39:** 217–226.

TAYLOR, A. H., R. J. GEIDER, AND F. J. H. GILBERT. 1997. Seasonal and latitudinal dependencies of phytoplankton carbon-to-chlorophyll *a* ratios: Results of a modelling study. Mar. Ecol. Prog. Ser. **152:** 51–66.

VENRICK, E. L. 1982. Phytoplankton in an oligotrophic ocean: Observations and questions. Ecol. Monogr. **52:** 129–154.

———, J. A. MCGOWAN, AND A. W. MANTYLA. 1973. Deep maxima of photosynthetic chlorophyll in the Pacific Ocean. Fish. Bull. **71:** 41–52.

VILLAREAL, T. A., M. A. ALTABET, AND K. CULVER-RYMSZA. 1993. Nitrogen transport by vertically migrating diatom mats in the North Pacific Ocean. Nature **363:** 709–712.

ZANEVELD, J. R. V. 1994. Optical closure: From theory to measurement, p. 59–72. *In* R. W. Spinrad, K. L. Carder, and M. J. Perry [eds.], Ocean optics. Oxford Monographs on Geology and Geophysics No. 25. Oxford Univ. Press.

Received: 5 June 2002
Accepted: 21 January 2003
Amended: 21 February 2003